Research Article GU J Sci, Part A, 11(3): 463-480 (2024) 10.54287/gujsa.1485920

Gazi University
Journal of Science
PART A: ENGINEERING AND INNOVATION
http://dergipark.org.tr/gujsa

Modeling Cardiovascular Flow with Artificial Viscosity: Analyzing Navier-Stokes Solutions and Simulating Cardiovascular Diseases

Hilal KARADAVUT[1] Gülnur HAÇAT[1,2*] Aytekin ÇIBIK[3]

[1] Gazi University, Graduate School of Natural and Applied Sciences, Ankara, Türkiye
[2] Yalova University, Department of Business Administration, Yalova, Türkiye
[3] Gazi University, Department of Mathematics, Ankara, Türkiye

Keywords

Artificial Viscosity
Cardiovascular Diseases
Finite Element Method
Navier-Stokes Equations

Abstract

In this paper, the numerical solutions of the Navier-Stokes equations (NSE) used for modeling the flow in the cardiovascular system are investigated using the Finite Element Method (FEM). A fully discrete solution scheme of the NSE and its stability and error analysis are presented. Artificial viscosity stabilization is added to the fully discrete scheme to better model the real flow structure and to remove non-physical oscillations. Numerical tests are also presented to demonstrate the effectiveness of the resulting scheme. Simulations analyzing the flow structure in the case of cardiovascular diseases such as atherosclerosis and brain aneurysm are presented in detail along with wall shear stress values.

Cite

Karadavut, H., Haçat, G., & Çıbık, A. (2024). Modeling Cardiovascular Flow with Artificial Viscosity: Analyzing Navier-Stokes Solutions and Simulating Cardiovascular Diseases. *GU J Sci, Part A, 11*(3), 463-480. doi:10.54287/gujsa.1485920

Author ID (ORCID Number)

0000-0003-1247-8004 Hilal KARADAVUT
0000-0001-7343-8466 Gülnur HAÇAT
0000-0003-3571-4137 Aytekin ÇIBIK

Article Process

Submission Date 17.05.2024
Revision Date 18.07.2024
Accepted Date 06.08.2024
Published Date 24.09.2024

1. INTRODUCTION

The cardiovascular system consists of three main components: blood, the heart that pumps blood to the body, and the vessels that distribute the pumped blood to the body. The cardiovascular system maintains the body's functions by transporting oxygen, nutrients and hormones to the body's cells and by removing waste products and carbon dioxide produced by the cells (Nair, 2017; Alimov, 2023). Cardiovascular diseases occur when impairments in the functions of the cardiovascular system affect blood circulation. Cardiovascular diseases are defined as disorders of the heart, blood vessels and blood function. These diseases can include vascular narrowing, blockage, weakening or widening, heart failure and stroke. According to the World Health Organization, cardiovascular diseases are the leading cause of death worldwide (WHO, 2017; Gaidai et al., 2023). Although statistics on cardiovascular disease provide data, a better understanding of the cardiovascular system is important.

Mathematical modeling and simulation of blood flow aim to better understand the conditions that influence the functioning of the system when cardiovascular diseases occur. The emergence of more powerful computers with improved image processing and geometry extraction techniques and the development of better algorithms have increased the demand for blood flow modeling among researchers (Formaggia et al., 2009; Taylor et al., 2023).

Mathematical models of blood flow can be divided into Newtonian models and non-Newtonian models. Newtonian models are models that neglect shear analysis and viscoelastic effects and can be applied to large vessels. Non-Newtonian models are those that take viscoelastic effects into account and can be applied to veins with a diameter of less than 1 mm. The non-Newtonian behavior makes the viscosity dependent on the shear

*Corresponding Author, e-mail: gulnur.yilmazoglu@yalova.edu.tr

rate, which increases the computational cost, so Newtonian models are usually used for simplicity. Therefore, models that exhibit Newtonian flow, such as the NSE, are often preferred to model blood flow in the cardiovascular system. The NSE is considered an important tool in understanding the movement of blood between vessels and its effects on the overall health of the system. The most general forms of these incompressible equations governing blood flow are as follows:

$$\begin{aligned} u_t + (u.\nabla)u - \nu\Delta u + \nabla p &= f, && (0,T]\times\Omega \\ \nabla.u &= 0 && (0,T]\times\Omega \\ u(x,0) &= u_0(x) && x\in\Omega \\ u &= 0 && \Gamma_{Wall} \\ n.\sigma &= 0 && \Gamma_{out} \\ u &= c && \Gamma_{in}\ . \end{aligned} \tag{1}$$

Here u represents the fluid velocity, p is the pressure, f is the force per unit mass of the fluid, ν the viscosity and σ the Cauchy stress tensor. Suppose that Ω represents a fluid domain and the boundaries of Ω consist of two distinct boundaries, Γ_{in} and Γ_{out}, with Γ_{Wall} representing the inner wall of the artery. The boundary of the section of the artery under consideration's input flow is denoted by Γ_{in}, and the border of its outflow flow by Γ_{out}. Neumann boundary condition on Γ_{out}, no-slip Dirichlet boundary condition on Γ_{Wall}, and Dirichlet boundary condition on Γ_{in} are all taken into consideration (Formaggia et al., 2009). Also, the function c, which stabilizes the input flow, is set as a parabolic function for the simulations.

Numerical solutions of these equations are used to understand the dynamics of blood flow, pressure changes in vessel walls and flow velocities (Quarteroni et al., 2002; Selmi et al., 2019; Ali et al., 2024). Besides the NSE, the most common method for the numerical solution of many partial differential equations is the finite element method, which involves dividing the domain into elements and approximating the solution as a linear combination of basis functions on these elements. In this formulation, large variations in some fluid properties can adversely affect the stability of numerical methods. Therefore, the artificial viscosity method is a technique used to provide stabilization in such cases. If the parameter of the method is chosen small, there is less artificial viscosity effect and more accurate results can be obtained with a better selection. On the other hand, if the parameter of the method is chosen larger, more artificial viscosity effects occur in the flow and the solution becomes more stable, but at the same time, more physical flow details may be lost. Therefore, a balanced selection of the parameter of the method is crucial to achieve accurate results. By stabilizing the fluid structure, artificial viscosity controls fluctuations and increases the stability of the numerical solution. Artificial viscosity techniques help CFD simulations produce more accurate results and predictions closer to real-world fluid dynamics (Manzari, 1999; Ma et al. 2022). In their work, Margolin and Lloyd-Ronning (2023) summarized the history of artificial viscosity, from its origins to current research and new directions for improvement. The work of Cook and Cabot (2005) has a similar structure.

Together with solutions of velocity, pressure fields and streamlines, we can calculate the wall shear stress (WSS=$\mu(du/dy)$) by analyzing the solution data. These data provide extremely valuable clues for understanding blood flow phenomena. Research shows that a continuous flow or oscillating shear stress can be signs of vessel anomalies, causing continuous damage to endothelial cells (Fisher et al., 2001; Chiu & Chien, 2011). However, measuring these stress values in a real patient can be quite challenging. This is where mathematical models and simulations can help us better understand real-world situations (Velten et al. 2024). These models can be integrated into the diagnosis and treatment of patients, thus contributing significantly to clinical practice and disease prognosis (Reneman & Hoeks, 2008; Formaggia et al., 2010; Arjmandi-Tash et al., 2011).

In this paper, a fully discretized scheme of NSE with artificial viscosity is introduced and numerical analysis and experiments are presented. In this context, after the necessary preliminaries in section 2, the stability and error analysis of the proposed scheme are presented in section 3. In section 4, numerical tests are performed to verify the accuracy of the theoretical results and simulations of cardiovascular conditions such as atherosclerosis and aneurysm are presented. In section 5, the benefits of the obtained results and future directions are discussed.

2. MATHEMATICAL PRELIMINARIES AND MATHEMATICAL MODELING

Since the FEM is used, the standard function spaces for the velocity field and pressure spaces are selected as follows (Adams, 1975):

$X = H_0^1(\Omega)$, and $Q = L_0^2(\Omega)$.

Let V be a weak subspace of X, then

$V \coloneqq \{v \in X, (\nabla . q, v) = 0, \forall q \in Q\}$.

The dual norm of a function is given by

$$\|f\|_{-1} \coloneqq \sup_{v \in H_0^1(\Omega)} \frac{(f, v)}{\|\nabla v\|}.$$

For $(v, q) \in (X, Q)$, the weak form of the NSE to be used is given below:

$$(u_t, v) + \nu(\nabla u, \nabla v) + b(u, u, v) - (p, \nabla . v) + (\nabla . u, q) = (f, v). \quad (2)$$

The nonlinear term in equation (2) is expressed in the following skew-symmetric trilinear forms:

$$b(u, v, w) \coloneqq \frac{1}{2}\big((u.\nabla)v, w\big) - \frac{1}{2}\big((u.\nabla)w, v\big). \quad (3)$$

Below are some properties of b that will be used later in error analysis.

Lemma 2.1. For $u, v, w \in X, b(u, v, w)$ satisfies the following bounds:

$$|b(u, v, w)| \leq C_0(\Omega)\|\nabla u\|\|\nabla v\| \, \|\nabla w\|, \quad (4)$$

$$|b(u, v, w)| \leq C_0(\Omega)\|u\|^{\frac{1}{2}}\|\nabla u\|^{\frac{1}{2}}\|\nabla v\| \, \|\nabla w\|.$$

Proof: The first inequality is obtained by taking the absolute value of the skew-symmetric trilinear form and making use of Cauchy-Schwarz and Poincare-Friedrich inequalities and similar arguments work for the second inequality too (Layton, 2008).

The application of the finite element method for spatial discretization requires the construction of a triangulation π_h of the domain Ω with maximum diameter h. Finite element spaces as given follows:

$X^h \subset X$ and $Q^h \subset Q$.

Lemma 2.2. It is assumed that the appropriate finite element spaces of velocity and pressure spaces satisfy the discrete inf-sup condition, i.e. the Ladyzenskaya-Brezzi-Babuska (LBB) condition. For example, let β be a constant, then

$$\inf_{v \in X^h} \sup_{q \in Q^h} \frac{(q^h, \nabla . v^h)}{\|\nabla v^h\|\|q^h\|} \geq \beta > 0.$$

We introduce the discretely divergence-free subspace $V^h \subset X^h$ given by

$$V^h \coloneqq \{v^h \in X^h, \big(\nabla . q^h, v^h\big) = 0, \forall q^h \in Q^h\}.$$

Under the inf-sup condition, V^h is a nonempty, closed subspace of X^h and the formulation in X^h is equivalent to V^h (John, 2004).

It is also assumed that the velocity and pressure finite element spaces satisfy the following well-known approximation properties (Layton, 2008):

$$\inf_{v\in X_h}\left(\|u-v^h\|+h\|\nabla(u-v^h)\|\right)\le Ch^{k+1}\|u\|_{k+1}\ ,\qquad u\in H^{k+1}(\Omega), \tag{4}$$

$$\inf_{q\in Q_h}\|p-q^h\|\le Ch^{s+1}\|p\|_{s+1}\ ,\qquad p\in H^{s+1}(\Omega).$$

for $(v^h,q^h)\in(X^h,Q^h)$.

Discrete Gronwall's inequality will be used in the error analysis (Girault & Raviart, 1979).

Lemma 2.3. (Discrete Gronwall's inequality) For $n\ge 0$ and $a_n,\ b_n,\ c_n,d_n,e_n$ be non-negative integers. If

$$a_{N+1}+\Delta t\sum_{n=0}^{N+1}b_n\le\Delta t\sum_{n=0}^{N+1}a_nd_n+\Delta t\sum_{n=0}^{N+1}c_n+H,\qquad N\ge 0$$

holds, then

$$a_{N+1}+\Delta t\sum_{n=0}^{N+1}b_n\le exp\left(\Delta t\sum_{n=0}^{N+1}\frac{e_n}{1-ke_n}\right)\left(\Delta t\sum_{n=0}^{N+1}c_n+H\right),\quad N\ge 0$$

for $ke_n<1$.

The fully discretized finite element approximation of the model is given below.

Algorithm 2.1: Given u_n^h, find $u_{n+1}^h\in X^h$satisfying:

$$\left(\frac{u_{n+1}^h-u_n^h}{\Delta t},v^h\right)+\nu\left(\nabla u_{n+1}^h,\nabla v^h\right)+b\left(u_{n+1}^h,u_{n+1}^h,v^h\right)-\left(p_{n+1}^h,\nabla.v^h\right)+\alpha\left(\nabla u_{n+1}^h,\nabla v^h\right)$$
$$=\left(f_{n+1},v^h\right), \tag{5}$$

$$\left(\nabla.u_{n+1}^h,q^h\right)=0,$$

where $\alpha\left(\nabla u_{n+1}^h,\nabla v^h\right)$ is the stabilization term that will increase the stability of the solution, representing the artificial viscosity, and α is the artificial viscosity parameter.

3. ANALYSIS OF THE SCHEME

This section focuses on the numerical analysis of Algorithm 2.1. In this context, the stability of the fully discrete approximation scheme is first analyzed. Then, the error analysis of the developed algorithm is performed.

3.1. Stability Analysis

Theorem 3.1: Let $f\in L^2(0,T;H^{-1}(\Omega))$. (5) is unconditionally stable and the solution found satisfies the following equation for any $h>0$ and $u^h,v^h\in X^h;\ p^h,q^h\in Q^h$:

$$\left\|u_N^h\right\|^2+\sum_{n=0}^{N-1}\Delta t\left(\frac{\nu}{2}+\alpha\right)\left\|\nabla u_{n+1}^h\right\|^2\le\left\|u_0^h\right\|^2+\sum_{n=0}^{N-1}\frac{\Delta t}{\nu}\|f_{n+1}\|_{-1}^2\ .$$

Proof: Given the schemes (5) on X^h, the equivalent formulation on V^h is

$$\left(\frac{u_{n+1}^h-u_n^h}{\Delta t}, v^h\right)+\nu\left(\nabla u_{n+1}^h, \nabla v^h\right)+b\left(u_{n+1}^h, u_{n+1}^h, v^h\right)+\alpha\left(\nabla u_{n+1}^h, \nabla v^h\right)=\left(f_{n+1}, v^h\right). \quad (7)$$

If $v^h=u_{n+1}^h$ is taken in (7), since $b\left(u_{n+1}^h, u_{n+1}^h, u_{n+1}^h\right)=0$ from (4), the equation becomes as follows:

$$\left(\frac{u_{n+1}^h-u_n^h}{\Delta t}, u_{n+1}^h\right)+\nu\left(\nabla u_{n+1}^h, \nabla u_{n+1}^h\right)+\alpha\left(\nabla u_{n+1}^h, \nabla u_{n+1}^h\right)=\left(f_{n+1}, u_{n+1}^h\right).$$

Here, we first multiply both sides of the equation by Δt and then rearrange the terms,

$$\left\|u_{n+1}^h\right\|^2+\Delta t(\nu+\alpha)\left\|\nabla u_{n+1}^h\right\|^2=\left(u_n^h, u_{n+1}^h\right)+\Delta t\left(f_{n+1}, u_{n+1}^h\right) \quad (8)$$

The terms on the right-hand side of the equation are analyzed separately. Using the Cauchy-Schwarz and Young's inequalities for the first term on the right, the following bound is obtained:

$$\left(u_n^h, u_{n+1}^h\right) \leq \left\|u_n^h\right\|\left\|u_{n+1}^h\right\| \leq \frac{1}{2}\left\|u_n^h\right\|^2+\frac{1}{2}\left\|u_{n+1}^h\right\|^2.$$

For the second term, the definition of dual norm is applied first, followed by Cauchy-Schwarz and Young inequalities respectively:

$$\begin{aligned}\Delta t\left(f_{n+1}, u_{n+1}^h\right) &= \frac{\Delta t\left(f_{n+1}, u_{n+1}^h\right)}{\left\|\nabla u_{n+1}^h\right\|}\left\|\nabla u_{n+1}^h\right\| \leq \Delta t\|f_{n+1}\|_{-1}\left\|\nabla u_{n+1}^h\right\| \\ &\leq \frac{\Delta t \nu}{2}\left\|\nabla u_{n+1}^h\right\|^2+\frac{1}{2\nu}\Delta t\|f_{n+1}\|_{-1}^2.\end{aligned}$$

Substituting the calculated terms in equation (8) yields the following inequality

$$\frac{1}{2}\left\|u_{n+1}^h\right\|^2+\Delta t\left(\frac{\nu}{2}+\alpha\right)\left\|\nabla u_{n+1}^h\right\|^2 \leq \frac{1}{2}\left\|u_n^h\right\|^2+\frac{\Delta t}{2\nu}\|f_{n+1}\|_{-1}^2.$$

If we take the sum for $n=0,1,\ldots,N-1$, we get

$$\left\|u_N^h\right\|^2+\sum_{n=0}^{N-1}\Delta t\left(\frac{\nu}{2}+\alpha\right)\left\|\nabla u_{n+1}^h\right\|^2 \leq \left\|u_0^h\right\|^2+\sum_{n=0}^{N-1}\frac{\Delta t}{\nu}\|f_{n+1}\|_{-1}^2$$

Then the inequality in Theorem 3.1 is obtained.

3.2. Error Analysis

In addition to the discrete inf-sup condition, the approximations in Lemma (2.2) are assumed to be valid for the selection of velocity-pressure spaces. First, we state the regularity assumptions required for NSE solutions.

$$u \in L^4\left(0,T;H^{k+1}(\Omega)\right)\cap L^4\left(0,T;L^2(\Omega)\right)\cap L^\infty\left(0,T;L^2(\Omega)\right),$$

$$p \in L^2\left(0,T;H^{s+1}(\Omega)\right),$$

$$u_t \in L^\infty\left(0,T;L^2(\Omega)\right).$$

Theorem 3.2: Let (u,p) be a solution of the NSE (1). Then the error of (5) defined as $e_{n+1}=u_{n+1}-u_{n+1}^h$ satisfies the following inequality:

$$\left\|e_N^h\right\|^2+\Delta t(\nu+\alpha)\sum_{n=0}^{N-1}\left\|\nabla e_{n+1}^h\right\|^2$$

$$\leq exp(\,C\nu^{-3}\Delta t\|\nabla u_{n+1}\|^4)\Big[C\nu^{-1}\Delta t\textstyle\sum_{n=0}^{N-1}\Big((\Delta t)^{-1}h^{2k+2}\int_{t_n}^{t_{n+1}}\|u_t\|_{k+1}^2dt+h^{2k}\|\nabla u_{n+1}\|^2\|u\|_{k+1}^2+$$
$$h^{2k}\left\|\nabla u_{n+1}^h\right\|^2\|u\|_{k+1}^2+h^{2k}\|p_{n+1}\|_k^2+(\Delta t)^2\int_{t_n}^{t_{n+1}}\|u_{tt}\|^2dt+(\Delta t)^3\int_{t_n}^{t_{n+1}}\|u_{tt}\|^2dt(\|\nabla u_{n+1}\|^2+$$
$$\|\nabla u\|^2)+(\Delta t)^3\int_{t_n}^{t_{n+1}}\|p_{tt}\|^2dt+(\Delta t)^3\int_{t_n}^{t_{n+1}}\|f_{tt}\|^2dt\Big)+C\nu\Delta th^{2k}\|u\|_{k+1}^2+C\nu(\Delta t)^4\|\nabla u_{tt}\|^2+$$
$$\alpha\Delta t\big(h^{2k}\|u\|_{k+1}^2+\|\nabla u_{n+1}\|^2\big)\Big].$$

Proof: The difference between the true solution and the approximate solution is estimated to obtain the minimum error. The equation

$$\Big(\frac{u_{n+1}-u_n}{\Delta t},v^h\Big)+\nu\big(\nabla u_{n+1},\nabla v^h\big)+b\big(u_{n+1},u_{n+1},v^h\big)-\big(p_{n+1},\nabla.v^h\big)+\big(\nabla.u_{n+1},q^h\big)+\alpha\big(\nabla u_{n+1},\nabla v^h\big)$$
$$-\alpha\big(\nabla u_{n+1},\nabla v^h\big)=\big(f_{n+1},v^h\big) \tag{9}$$

is obtained by writing $t\to t_{n+1}$ in the true solution of (1) and adding and subtracting the $\alpha\big(\nabla u_{n+1},\nabla v^h\big)$ term. Subtract (5) from (9),

$$\Big(\frac{e_{n+1}-e_n}{\Delta t},v^h\Big)+\nu\big(\nabla e_{n+1},\nabla v^h\big)+b\big(u_{n+1},u_{n+1},v^h\big)-b\big(u_{n+1}^h,u_{n+1}^h,v^h\big)-\big(p_{n+1}-q^h,\nabla.v^h\big)$$
$$+\alpha\big(\nabla e_{n+1},\nabla v^h\big)=\tau\big(u_n,v^h\big) \tag{10}$$

where $e_{n+1}=u_{n+1}-u_{n+1}^h$. The nonlinear terms on the right side of (10) can be arranged as follows:

$$b\big(u_{n+1},u_{n+1},v^h\big)-b\big(u_{n+1}^h,u_{n+1}^h,v^h\big)$$

$$=\ b\big(u_{n+1},u_{n+1},v^h\big)-b\big(u_{n+1}^h,u_{n+1},v^h\big)+b\big(u_{n+1}^h,u_{n+1},v^h\big)-b\big(u_{n+1}^h,u_{n+1}^h,v^h\big)$$

$$=b\big(e_{n+1},u_{n+1},v^h\big)-b\big(u_{n+1}^h,e_{n+1},v^h\big).$$

The error can be decomposed as

$$e_{n+1}=u_{n+1}-\tilde{u}_{n+1}+\tilde{u}_{n+1}-u_{n+1}^h=\mu_{n+1}-\emptyset_{n+1}^h,$$

where $\tilde{u}_{n+1}$ is the arbitrary interpolant. Choosing the test function $v^h=\emptyset_{n+1}^h$ yields

$$\left(\frac{\emptyset_{n+1}^h-\emptyset_n^h}{\Delta t},\emptyset_{n+1}^h\right)+\nu\big(\nabla\emptyset_{n+1}^h,\nabla\emptyset_{n+1}^h\big)+b\big(\emptyset_{n+1}^h,u_{n+1},\emptyset_{n+1}^h\big)+\big(p_{n+1}-q^h,\nabla.\emptyset_{n+1}^h\big)$$

$$+\alpha\big(\nabla\emptyset_{n+1}^h,\nabla\emptyset_{n+1}^h\big)$$

$$=\Big(\frac{\mu_{n+1}-\mu_n}{\Delta t},\emptyset_{n+1}^h\Big)+\nu\big(\nabla\mu_{n+1},\nabla\emptyset_{n+1}^h\big)+b\big(\mu_{n+1},u_{n+1},\emptyset_{n+1}^h\big)+b\big(u_{n+1}^h,\mu_{n+1},\emptyset_{n+1}^h\big)$$

$$+\alpha\big(\nabla\mu_{n+1},\nabla\emptyset_{n+1}^h\big)+\tau\big(u_n,\nabla\emptyset_{n+1}^h\big).$$

Here,

$$\tau(u_n,\nabla\emptyset_{n+1}^h)=\left(\frac{u_{n+1}-u_n}{\Delta t}-u_t,\emptyset_{n+1}^h\right)-(p_{n+1}-p,\nabla.\emptyset_{n+1}^h)+(f-f_{n+1},\emptyset_{n+1}^h)$$
$$+\nu(\nabla(u_{n+1}-u_n),\nabla\emptyset_{n+1}^h)+b(u_{n+1}-u_n,u_{n+1},\emptyset_{n+1}^h)+b(u,u_{n+1}-u,\emptyset_{n+1}^h)$$
$$+\alpha\left(\nabla u_{n+1},\nabla\emptyset_{n+1}^h\right).$$

Using the equation $a^2-ab=\frac{a^2+(a-b)^2-b^2}{2}$, the first term is organized as follows:

$$(\emptyset_{n+1}^h-\emptyset_n^h,\emptyset_{n+1}^h)=\frac{1}{2}\left(\|\emptyset_{n+1}^h\|^2+\|\emptyset_{n+1}^h-\emptyset_n^h\|^2-\|\emptyset_n^h\|^2\right).$$

Accordingly,

$$\frac{1}{2\Delta t}\left(\|\emptyset_{n+1}^h\|^2+\|\emptyset_{n+1}^h-\emptyset_n^h\|^2-\|\emptyset_n^h\|^2\right)+\nu\|\nabla\emptyset_{n+1}^h\|^2+\alpha\|\nabla\emptyset_{n+1}^h\|^2$$
$$=\left(\frac{\mu_{n+1}-\mu_n}{\Delta t},\emptyset_{n+1}^h\right)+\nu(\nabla\mu_{n+1},\nabla\emptyset_{n+1}^h)+b(\mu_{n+1},u_{n+1},\emptyset_{n+1}^h)+b(u_{n+1}^h,\mu_{n+1},\emptyset_{n+1}^h)$$
$$-b(\emptyset_{n+1}^h,u_{n+1},\emptyset_{n+1}^h)-(p_{n+1}-q^h,\nabla.\emptyset_{n+1}^h)+\alpha(\nabla\mu_{n+1},\nabla\emptyset_{n+1}^h)+\tau(u_n,\nabla\emptyset_{n+1}^h)$$
$$=T_1+T_2+\cdots+T_8. \tag{11}$$

Here, the terms obtained on the right side of the equation are named $T_1,T_2,\dots,T_8$ respectively. Each term will be analyzed separately, and necessary adjustments will be made.

T_1 is bounded by Cauchy-Schwarz, and Young's inequalities:

$$\left(\frac{\mu_{n+1}-\mu_n}{\Delta t},\emptyset_{n+1}^h\right)\le\frac{1}{\Delta t}\left\|\int_{t_n}^{t_{n+1}}\mu_t dt\right\|\|\emptyset_{n+1}^h\|\le\frac{C\nu^{-1}}{\Delta t}\int_{t_n}^{t_{n+1}}\|\mu_t\|^2dt+\frac{\nu}{24}\|\nabla\emptyset_{n+1}^h\|^2.$$

T_2 is bounded by Young's inequalities:

$$\nu(\nabla\mu_{n+1},\nabla\emptyset_{n+1}^h)\le C\nu\|\nabla\mu_{n+1}\|^2+\frac{\nu}{24}\|\nabla\emptyset_{n+1}^h\|^2.$$

For T_3, T_4, and T_5 first apply Lemma 2.2, then Young's inequality to get:

$$b(\mu_{n+1},u_{n+1},\emptyset_{n+1}^h)\le C\nu^{-1}\|\nabla u_{n+1}\|^2\|\nabla\mu_{n+1}\|^2+\frac{\nu}{24}\|\nabla\emptyset_{n+1}^h\|^2,$$

$$b(u_{n+1}^h,\mu_{n+1},\emptyset_{n+1}^h)\le C\nu^{-1}\|\nabla u_{n+1}^h\|^2\|\nabla\mu_{n+1}\|^2+\frac{\nu}{24}\|\nabla\emptyset_{n+1}^h\|^2,$$

$$b(\emptyset_{n+1}^h,u_{n+1},\emptyset_{n+1}^h)\le C\nu^{-3}\|\emptyset_{n+1}^h\|^2\|\nabla u_{n+1}\|^4+\frac{\nu}{24}\|\nabla\emptyset_{n+1}^h\|^2.$$

Young's inequality is applied for T_6, T_7, and T_8

$$(p_{n+1}-q^h,\nabla.\emptyset_{n+1}^h)\le C\nu^{-1}\|p_{n+1}-q^h\|^2+\frac{\nu}{24}\|\nabla\emptyset_{n+1}^h\|^2,$$

$$\alpha(\nabla\mu_{n+1},\nabla\emptyset_{n+1}^h)\le C\alpha\|\nabla\mu_{n+1}\|^2+\frac{\alpha}{4}\|\nabla\emptyset_{n+1}^h\|^2.$$

The terms given in equation T_8=$\tau(u_n,\nabla\emptyset_{n+1}^h)$ are named $S_1,S_2,\dots,S_7$ and analyzed separately.

$$\tau(u_n,\nabla\emptyset_{n+1}^h)=\left(\frac{u_{n+1}-u_n}{\Delta t}-u_t,\emptyset_{n+1}^h\right)+\nu\left(\nabla(u_{n+1}-u),\nabla\emptyset_{n+1}^h\right)+b\left(u_{n+1}-u_n,u_{n+1},\emptyset_{n+1}^h\right)$$
$$+b\left(u,u_{n+1}-u,\emptyset_{n+1}^h\right)-\left(p_{n+1}-p,\nabla.\emptyset_{n+1}^h\right)+\left(f-f_{n+1},\emptyset_{n+1}^h\right)$$
$$=S_1+S_2+\cdots+S_7.$$

Taylor Series expansion and Young's inequality are applied for these terms:

$$\left(\frac{u_{n+1}-u_n}{\Delta t}-u_t,\emptyset_{n+1}^h\right)\le C\nu^{-1}(\Delta t)^2\int_{t_n}^{t_{n+1}}\|u_{tt}\|^2dt+\frac{\nu}{24}\left\|\nabla\emptyset_{n+1}^h\right\|^2,$$

$$\nu\left(\nabla(u_{n+1}-u),\nabla\emptyset_{n+1}^h\right)\le C\nu\|\nabla(u_{n+1}-u)\|^2+\frac{\nu}{24}\left\|\nabla\emptyset_{n+1}^h\right\|^2\le C\nu(\Delta t^3)\int_{t_n}^{t_{n+1}}\|\nabla u_{tt}\|^2dt+\frac{\nu}{24}\left\|\nabla\emptyset_{n+1}^h\right\|^2,$$

$$b\left(u_{n+1}-u_n,u_{n+1},\emptyset_{n+1}^h\right)\le C\nu^{-1}(\Delta t)^3\|\nabla u_{n+1}\|^2\int_{t_n}^{t_{n+1}}\|u_{tt}\|^2dt+\frac{\nu}{24}\left\|\nabla\emptyset_{n+1}^h\right\|^2,$$

$$b\left(u,u_{n+1}-u,\emptyset_{n+1}^h\right)\le C\nu^{-1}(\Delta t)^3\|\nabla u\|^2\int_{t_n}^{t_{n+1}}\|u_{tt}\|^2dt+\frac{\nu}{24}\left\|\nabla\emptyset_{n+1}^h\right\|^2,$$

$$\left(p_{n+1}-p,\nabla.\emptyset_{n+1}^h\right)\le C\nu^{-1}(\Delta t)^3\int_{t_n}^{t_{n+1}}\|p_{tt}\|^2dt+\frac{\nu}{24}\left\|\nabla\emptyset_{n+1}^h\right\|^2,$$

$$\left(f-f_{n+1},\emptyset_{n+1}^h\right)\le C\nu^{-1}\|f-f_{n+1}\|^2+\frac{\nu}{24}\left\|\nabla\emptyset_{n+1}^h\right\|^2\le C\nu^{-1}(\Delta t)^3\int_{t_n}^{t_{n+1}}\|f_{tt}\|^2dt+\frac{\nu}{24}\left\|\nabla\emptyset_{n+1}^h\right\|^2,$$

$$\alpha\left(\nabla u_{n+1},\nabla\emptyset_{n+1}^h\right)\le C\alpha\|\nabla u_{n+1}\|^2+\frac{\alpha}{4}\left\|\nabla\emptyset_{n+1}^h\right\|^2.$$

Substituting all the terms obtained in (11) and subtracting the non-negative term on the left side of the equation gives

$$\frac{1}{2\Delta t}\left\|\emptyset_{n+1}^h\right\|^2-\frac{1}{2\Delta t}\left\|\emptyset_n^h\right\|^2+\frac{\nu}{2}\left\|\nabla\emptyset_{n+1}^h\right\|^2+\frac{\alpha}{2}\left\|\nabla\emptyset_{n+1}^h\right\|^2$$
$$\le C\nu^{-1}\Bigg[(\Delta t)^{-1}\int_{t_n}^{t_{n+1}}\|\mu_t\|^2dt+\|\nabla u_{n+1}\|^2\|\nabla\mu_{n+1}\|^2+\left\|\nabla u_{n+1}^h\right\|^2\|\nabla\mu_{n+1}\|^2$$
$$+\left\|p_{n+1}-q^h\right\|^2+(\Delta t)^2\int_{t_n}^{t_{n+1}}\|u_{tt}\|^2dt+(\Delta t)^3\int_{t_n}^{t_{n+1}}\|u_{tt}\|^2dt(\|\nabla u_{n+1}\|^2+\|\nabla u\|^2)$$
$$+(\Delta t)^3\int_{t_n}^{t_{n+1}}\|p_{tt}\|^2dt+(\Delta t)^3\int_{t_n}^{t_{n+1}}\|f_{tt}\|^2dt\Bigg]+C\nu\|\nabla\mu_{n+1}\|^2+C\nu^{-3}\left\|\emptyset_{n+1}^h\right\|^2\|\nabla u_{n+1}\|^4$$
$$+C\alpha(\|\nabla\mu_{n+1}\|^2+\|\nabla u_{n+1}\|^2)+C\nu(\Delta t^3)\int_{t_n}^{t_{n+1}}\|\nabla u_{tt}\|^2dt$$

Multiplying inequality by 2Δt and applying Lemma 2.2 yields the following:

$$\begin{aligned}
&\left\|\emptyset_{n+1}^{h}\right\|^2-\left\|\emptyset_{n}^{h}\right\|^2+\Delta t(\nu+\alpha)\left\|\nabla\emptyset_{n+1}^{h}\right\|^2\\
&\qquad\leq C\nu^{-1}\Delta t\Bigg[(\Delta t)^{-1}h^{2k+2}\int_{t_n}^{t_{n+1}}\|u_t\|_{k+1}^2dt+h^{2k}\|\nabla u_{n+1}\|^2\|u\|_{k+1}^2+h^{2k}\left\|\nabla u_{n+1}^{h}\right\|^2\|u\|_{k+1}^2\\
&\qquad+h^{2k}\|p_{n+1}\|_k^2+(\Delta t)^2\int_{t_n}^{t_{n+1}}\|u_{tt}\|^2dt+(\Delta t)^3\int_{t_n}^{t_{n+1}}\|u_{tt}\|^2dt(\|\nabla u_{n+1}\|^2+\|\nabla u\|^2)\\
&\qquad+(\Delta t)^3\int_{t_n}^{t_{n+1}}\|p_{tt}\|^2dt+(\Delta t)^3\int_{t_n}^{t_{n+1}}\|f_{tt}\|^2dt\Bigg]+C\nu\Delta th^{2k}\|u\|_{k+1}^2\\
&\qquad+\ C\nu^{-3}\Delta t\left\|\emptyset_{n+1}^{h}\right\|^2\|\nabla u_{n+1}\|^4+\alpha\Delta t\left(h^{2k}\|u\|_{k+1}^2+\|\nabla u_{n+1}\|^2\right)\\
&\qquad+C\nu(\Delta t^3)\Delta t\int_{t_n}^{t_{n+1}}\|\nabla u_{tt}\|^2dt
\end{aligned}$$

If the sum is taken for $n=0,1,\dots,N-1$, we obtain

$$\begin{aligned}
&\left\|\emptyset_{N}^{h}\right\|^2+\Delta t(\nu+\alpha)\sum_{n=0}^{N-1}\left\|\nabla\emptyset_{n+1}^{h}\right\|^2\\
&\qquad\leq\Bigg[C\nu^{-1}\Delta t\sum_{n=0}^{N-1}\Bigg((\Delta t)^{-1}h^{2k+2}\int_{t_n}^{t_{n+1}}\|u_t\|_{k+1}^2dt+h^{2k}\|\nabla u_{n+1}\|^2\|u\|_{k+1}^2\\
&\qquad+h^{2k}\left\|\nabla u_{n+1}^{h}\right\|^2\|u\|_{k+1}^2+h^{2k}\|p_{n+1}\|_k^2+(\Delta t)^2\int_{t_n}^{t_{n+1}}\|u_{tt}\|^2dt\\
&\qquad+(\Delta t)^3\int_{t_n}^{t_{n+1}}\|u_{tt}\|^2dt(\|\nabla u_{n+1}\|^2+\|\nabla u\|^2)+(\Delta t)^3\int_{t_n}^{t_{n+1}}\|p_{tt}\|^2dt+(\Delta t)^3\int_{t_n}^{t_{n+1}}\|f_{tt}\|^2dt\Bigg)\\
&\qquad+C\nu\Delta th^{2k}\|u\|_{k+1}^2+C\nu(\Delta t)^4\|\nabla u_{tt}\|^2\\
&\qquad+\alpha\Delta t\left(h^{2k}\|u\|_{k+1}^2+\|\nabla u_{n+1}\|^2\right)\Bigg]exp(\ C\nu^{-3}\Delta t\|\nabla u_{n+1}\|^4)
\end{aligned}$$

Finally, Theorem 3.2 is obtained by applying the triangle inequality $\|e_{n+1}\|=\left\|\mu_{n+1}-\emptyset_{n+1}^{h}\right\|\leq\|\mu_{n+1}\|+\left\|\emptyset_{n+1}^{h}\right\|$ to the error terms using approximation properties.

Result 3.1: The error approximation obtained in Theorem 3.2 is an optimal error approximation. For example, if $k=2$, the order of the error according to the polynomial choices (P^2,P^1) is 2. It is also clear from the statement of the theorem that $u\to u_h$ when $h,\Delta t,\alpha\to 0$.

4. NUMERICAL SIMULATION

In this section, some simulations are presented to verify the theoretical results. Firstly, a quantitative numerical test is carried out to reveal the convergence behavior of the scheme in (5) and to verify the result obtained in Theorem 1. In qualitative experiments, blood and body temperature are assumed to be constant. For the understanding of blood flow, blood is assumed to be a Newtonian fluid. Therefore, blood density ρ=1060 kg/m3 and blood viscosity ν=0.0035 mPas were chosen (Kleinstreuer, 2016). A no-slip boundary condition is applied to the artery walls. Also, to determine the blood flow velocity, $c=\nu Re/\rho l$ is taken as the inflow

velocity, where l is the diameter of the lumen. The value of c is important to estimate the velocity at a specific point of blood flow or to analyze the overall performance of blood vessels. In this paper, all simulations were performed using FreeFem++ (Hecht., 2012), a publicly licensed finite element software package.

4.1. Convergence Study

First, the order of the spatial error is analyzed. Since the Taylor-Hood finite element pair mentioned in Result 1 is considered here, the expected order of the error is 2. The model problem computational domain is $\Omega = (0,1)^2$. The computational domain is triangulated with various coarse mesh resolutions and the mesh width is taken from $h = 2^{-1}$ to $h = 2^{-6}$. These choices were sufficient to verify the convergence rates. The converged solution was computed in the time interval [0, 1]. To minimize the effect of temporal error and to fully reveal the spatial effect on the error, $\Delta t = 0{,}000625$ was taken. The H_1 norms of the error for $\nu = 1$ and $\alpha = 0.01$ are evaluated. These values were optimally chosen to minimize the error rates in the newly derived model. For this test problem, the analytical velocity and pressure variables are considered as follows:

$$u = \begin{bmatrix} e^t cos(y) \\ e^t sin(x) \end{bmatrix}, p = (x - y)(1 + t).$$

These values are substituted in (1) and the function f is obtained. The results of the numerical solution are given in Table 1 for different values of h.

Table 1. *Spatial velocity errors and rates of convergence*

h	$\|\nabla(u - u^h)\|$	Rate
2^{-1}	6,46611e-4	-
2^{-2}	1,57286e-4	2,03
2^{-3}	3,85477e-5	2,02
2^{-4}	9,56907e-6	2,01
2^{-5}	2,38566e-6	2,00
2^{-6}	5,96731e-7	2,00

As can be seen from this table, the degree of convergence in the spatial sense is 2, which is the expected optimal degree of convergence. Similarly, in order to find the degree of temporal error, a fixed mesh size of $h = 2^{-6}$ was taken in the same region using the same true solution functions and the right-hand side. Δt values are halved iteratively in time interval [0, 1] to obtain a rate. The results are presented in Table 2.

Table 2. *Temporal velocity errors and rates of convergence*

Δt	$\|\nabla(u - u^h)\|$	Rate
2^{-1}	1,98947e-1	-
2^{-2}	1,70164e-2	3,55
2^{-3}	2,91767e-3	2,54
2^{-4}	2,17324e-4	1,98

The effect of the α stabilization term on the error rates calculated at different Re values for $h = 2^{-3}$ and $\Delta t = 0{,}125$ will be compared in Table 3.

Table 3. *Velocity errors for different α values*

Re	$\|\nabla(u - u^h)\|$ for $\alpha = 0$	$\|\nabla(u - u^h)\|$ for $\alpha = 0,01$
100	0,0903558	0,0797131
200	0,140067	0,11151
300	0,186865	0,134197
400	0,233123	0,151754
500	0,27908	0,165875

4.2. Study of Two-Necked Vessels

As a result of plaque formation in the vessel, knuckles, i.e. hardness, may occur on the upper and lower surfaces of the vessel in a reciprocal or non-reciprocal manner. This situation negatively affects the blood flow. In the numerical experiments, we tried to obtain the closest and most accurate solutions to the real blood flow with artificial viscosity stabilization. For this purpose, different Reynolds numbers were examined and the α's that would give the most accurate result were tuned.

As can be seen from Figure 1, artificial viscosity stabilization has a significant impact on the solution when analyzing the velocity of blood flow.

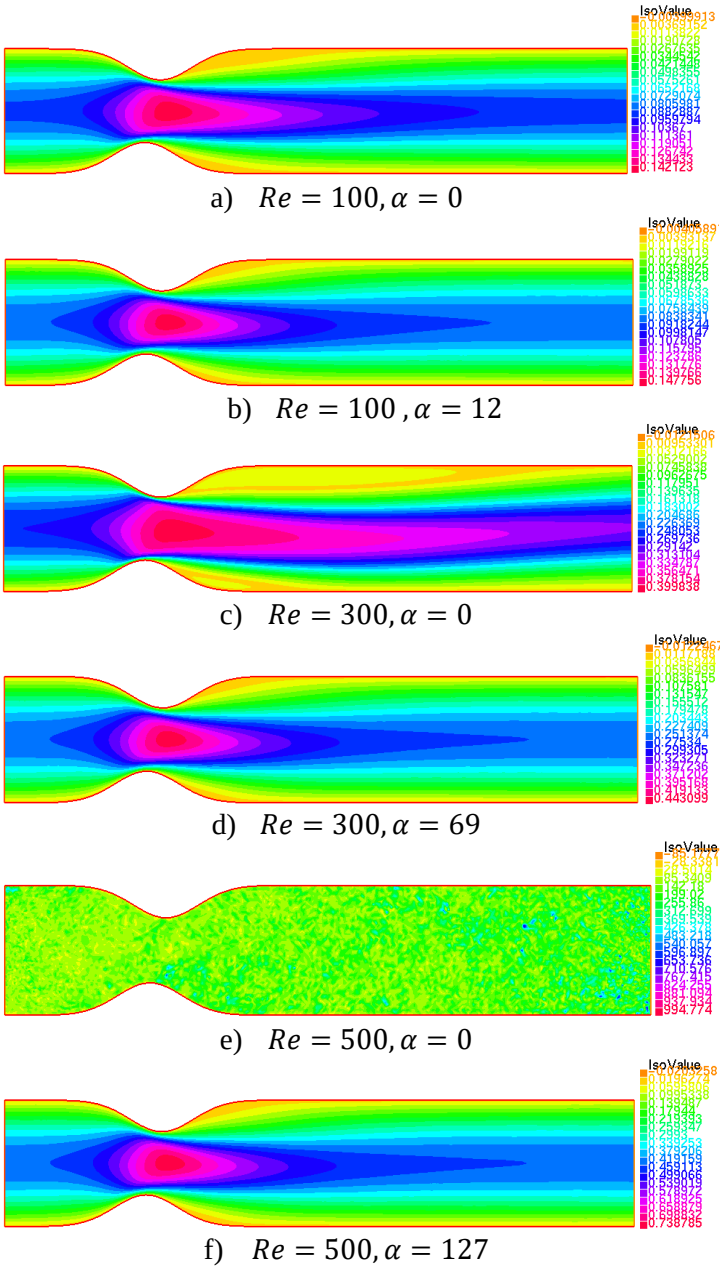

Figure 1. *Comparison of the effect of artificial viscosity stabilization for different values of the Reynolds number on the blood flow velocity in a two-necked vessel*

Figure 2 is important for understanding the effects of artificial viscosity stabilization on blood pressure. Determining how the pressure profile changes when blood flow has different Re and how artificial viscosity affects this profile can help in the development of better designed and effective medical devices and treatment

methods. Furthermore, this analysis can provide the necessary information to better model the behavior of blood flow in different conditions.

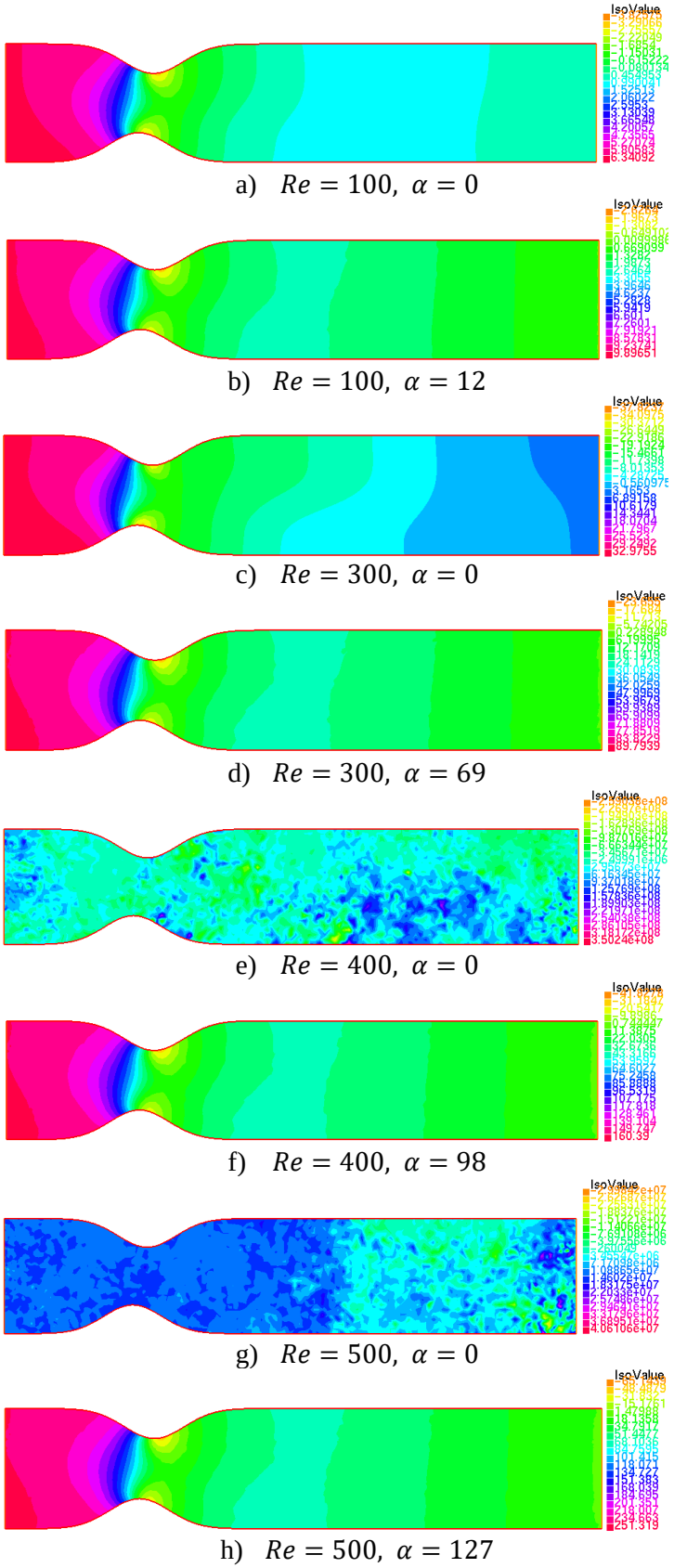

Figure 2. *Comparison of the effect of artificial viscosity stabilization for different values of Re on blood pressure in a two-necked vessel*

Figure 3 shows the errors at $Re = 500$ for different values of α to illustrate the effect of the stabilization.

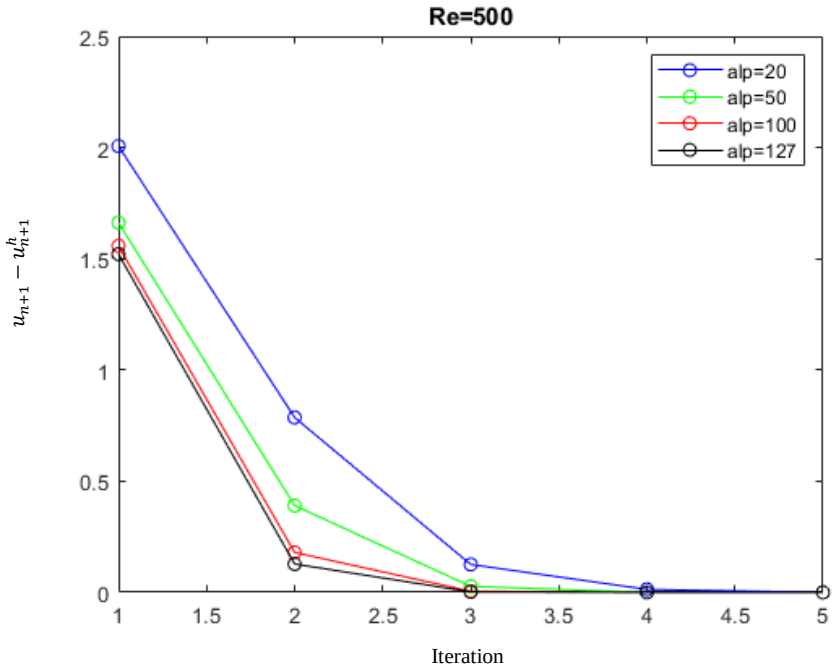

Figure 3. *Errors for different α values for Re=500*

For a given number Re, iterations are obtained with different α values. Considering the error rates resulting from these iterations, the α value that will give the minimum error is selected. As can be seen from the figure, for $Re = 500$, error rates were calculated considering different α values and it was seen that $\alpha = 127$ gave the minimum error.

4.3. Wall Shear Stress in Brain Aneurysm

Figure 4 shows the section focusing on WSS in a brain aneurysm. This figure shows simulation results using FreeFem++ software to model blood flow and its effects on the aneurysm.

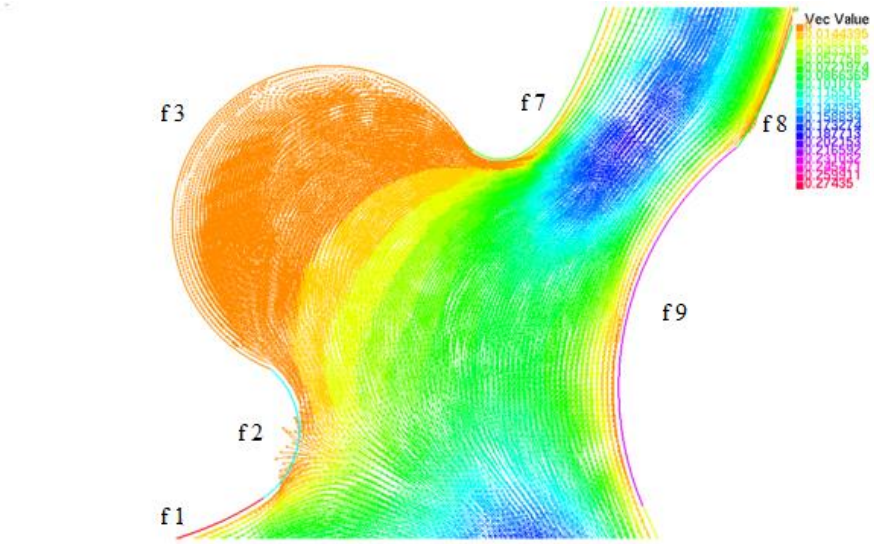

Figure 4. *FreeFem++ simulation of a brain aneurysm model*

Figures (5-10) of the regions with and without stabilization for $Re = 200$ and $\alpha = 205$ values are given below.

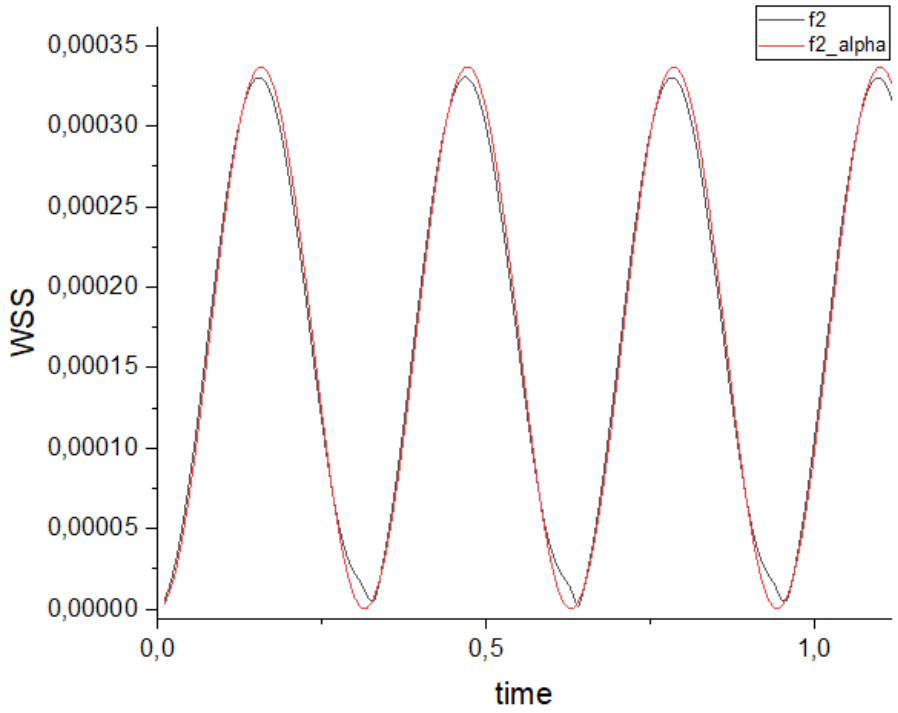

Figure 5. *WSS values for the f2 region*

The maximum WSS value in this region was approximately 0,000355 Pa, close to $\alpha = 0$. The flow in the vessels of the brain is usually pulsatile. This is caused by the expansion and contraction of the arteries with the beating of the heart. This is due to changes in the direction of blood flow in the inner walls of the arteries.

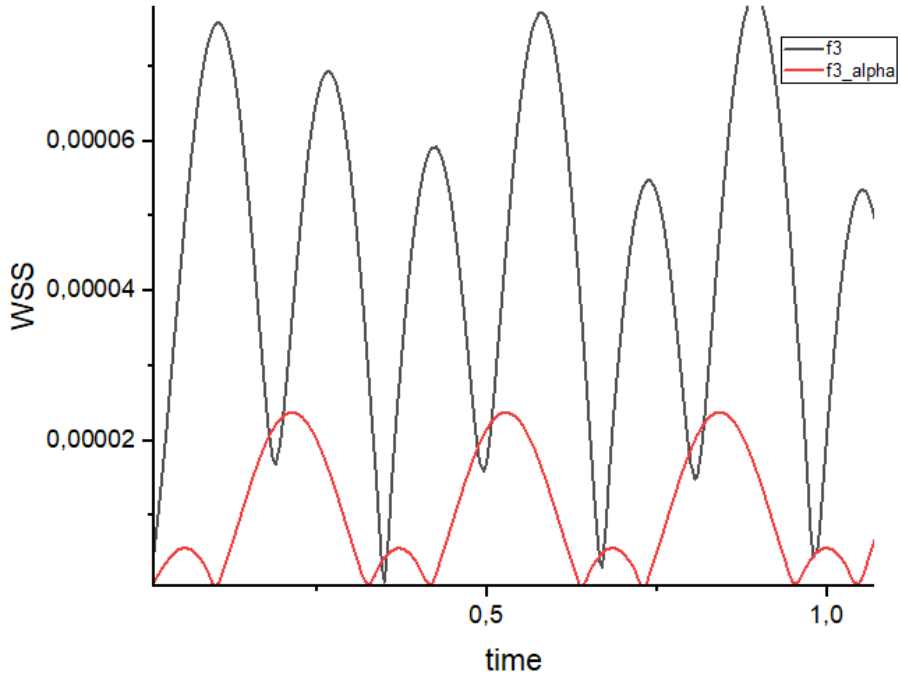

Figure 6. *WSS values for the f3 region*

As seen in the graph for the f3 region, it is clear that when there is no stabilization, results far from the general structure of the flow is obtained. The reason why the WSS value in this region is lower than f2 and f7 is due to the slowdown in the flow in these regions, as can be seen from the model (Figure 4).

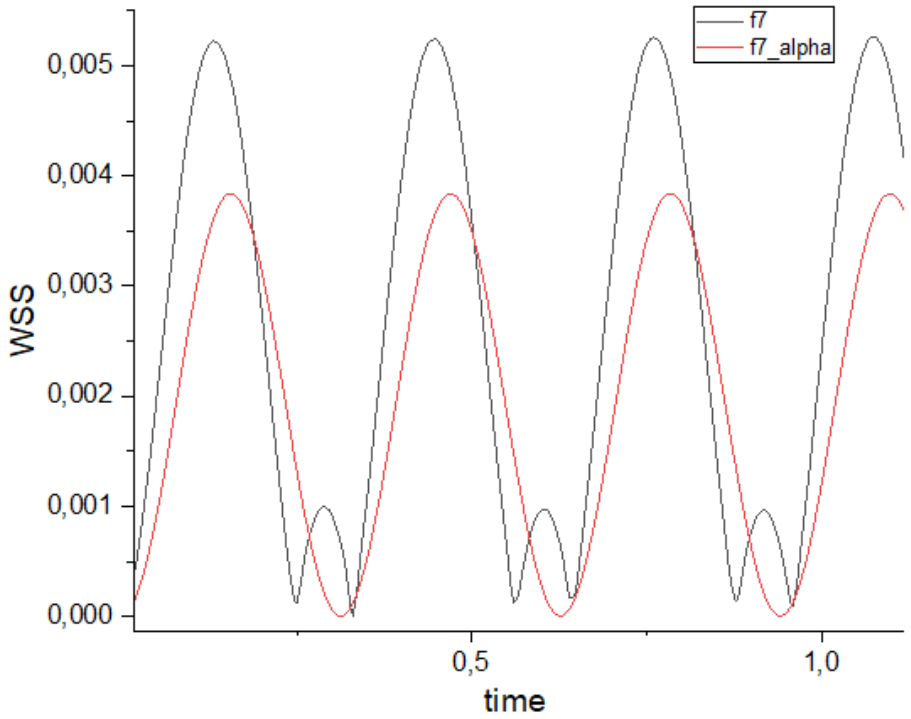

Figure 7. *WSS values for the f7 region*

The region where the WSS value is the highest, that is, the region where the stress is the highest, is the f7 region. This is because the flow is concentrated in this region and it contains the choke point.

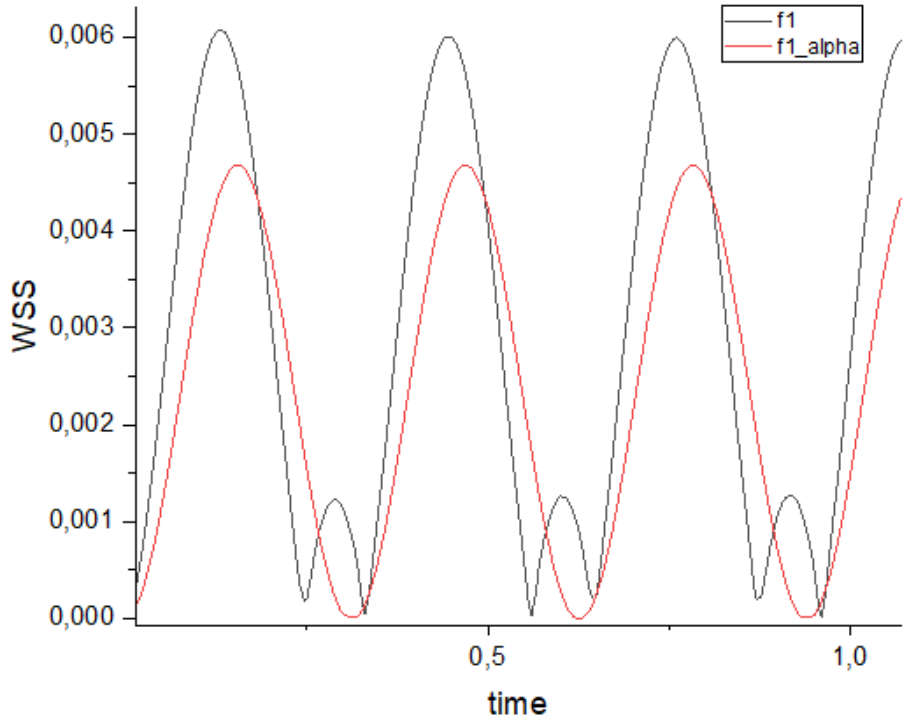

Figure 8. *WSS values for the f1 region*

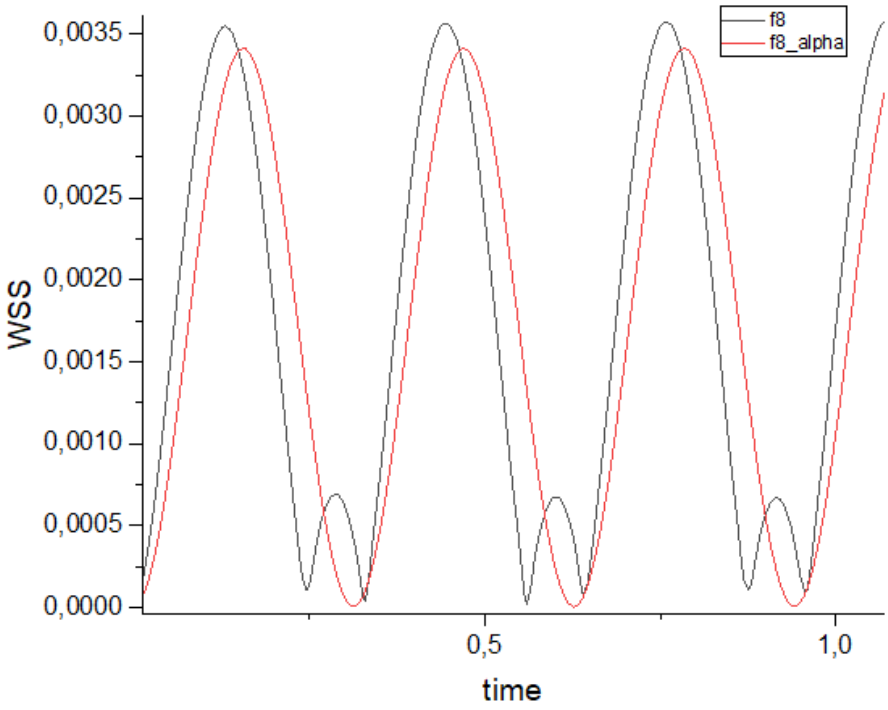

Figure 9. *WSS values for the f8 region*

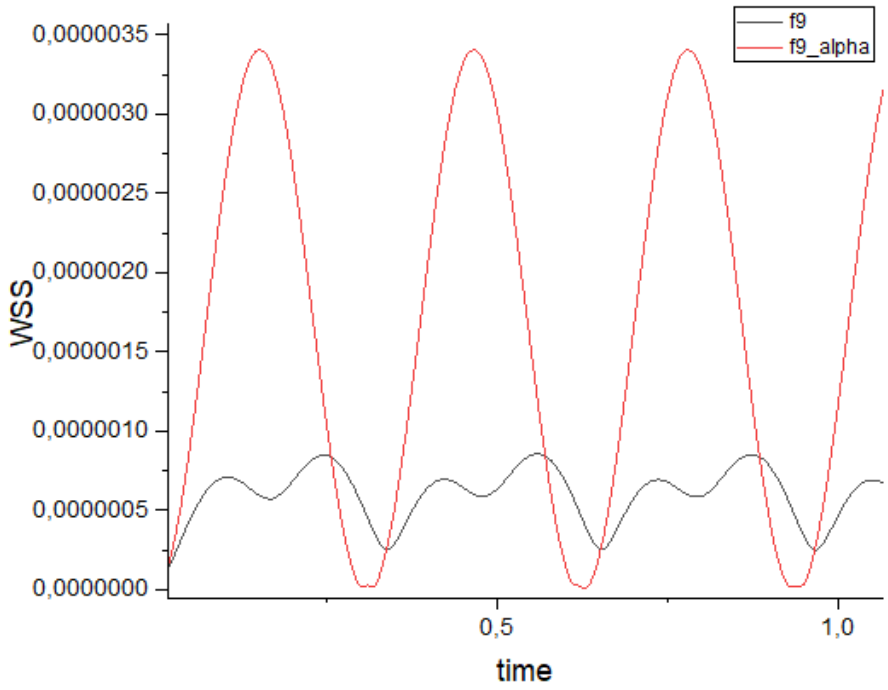

Figure 10. *WSS values for the f9 region*

When we examine the graphs of f1, f8 and f9 regions, it is in the f9 region that we will see the effect of stabilization the most. This is because the flow is in a more complex situation. As can be seen from f9 graph, when α is higher, the WSS values are more regular in accordance with the blood flow.

5. CONCLUSION

In this paper, changes in vascular flow due to cardiovascular diseases are analyzed with the NSE model. Stability and error analysis of the fully discrete scheme are performed. A stabilization term $\alpha(\nabla u, \nabla v)$

representing the artificial viscosity is used to stabilize the fully discrete finite element scheme. Numerical convergence tests are presented to verify the theoretical convergence rates, demonstrating the effectiveness of the proposed scheme. In addition, the effects of cardiovascular diseases on blood flow velocity, blood pressure and wall shear stress in vessels are modeled. Throughout the obtained models, it is shown how effective the scheme is and thanks to the stabilization, accurate, understandable and realistic results are obtained.

The results of this study provide a better understanding of the changes in blood flow in vessels caused by cardiovascular diseases. The analysis using the NSE model reveals the complexity of the dynamics in vessel flow and shows that these dynamics can be reliably modeled through stability and error analysis of the fully discrete scheme. The stabilization term representing the artificial viscosity improves the accuracy and stability of the model, making the results realistic and reliable. The verification of the theoretical convergence rates by numerical convergence tests reinforces the effectiveness of the proposed scheme and demonstrates the usability of this approach in practical applications. With this model, the effects of cardiovascular diseases on blood flow velocity, blood pressure and wall shear stress can be studied in detail and the effects of these parameters on disease progression can be better understood.

The results provide important information for planning medical interventions and disease management. The accuracy of the model and the reliable results provided by stabilization can contribute to the development of decision support systems in clinical applications. This could enable more efficient management of patients' treatment processes and early detection of diseases. Therefore, this study can be considered as an important step towards a better understanding and management of cardiovascular diseases.

AUTHOR CONTRIBUTIONS

Conceptualization, A.Ç.; methodology, A.Ç.; fieldwork, H. K.; software, A. Ç. and G.H.; title, G. H.; validation, A. Ç.; formal analysis, A. Ç. and G.H.; research, H. K.; sources, H. K.; manuscript-original draft, G.H.; manuscript-review and editing, A.Ç.; visualization, G.H.; supervision, A.Ç.

All authors have read and legally accepted the final version of the article published in the journal.

CONFLICT OF INTEREST

The authors declare no conflict of interest.

REFERENCES

Adams, R. A. (1975). *Sobolev Spaces*. Academic Press, New York.

Ali, S., Najjar, I. M. R., Sadoun, A. M., & Fathy, A. (2024). Navigating cardiovascular dynamics through mathematical modeling of arterial blood flow. *Ain Shams Engineering Journal*, *15*(4), 102594. https://doi.org/10.1016/j.asej.2023.102594

Alimov, N. (2023). Blood Supply to the Human Body, Vascular Anatomy and Blood Components. *Western European Journal of Medicine and Medical Science*, *1*(4), 4-14.

Arjmandi-Tash, O., Razavi, S. E., & Zanbouri, R. (2011). Possibility of atherosclerosis in an arterial bifurcation model. *BioImpacts*, *1*(4), 225-228. https://doi.org/10.5681/bi.2011.032

Chiu, J.-J., & Chien, S. (2011). Effects of disturbed flow on vascular endothelium: pathophysiological basis and clinical perspectives. *Physiological Reviews*, *91*(1), 327-387. https://doi.org/10.1152/physrev.00047.2009

Cook, A. W., & Cabot, W. H. (2005). Hyperviscosity for shock-turbulence interactions. *Journal of Computational Physics*, *203*(2), 379-385. https://doi.org/10.1016/j.jcp.2004.09.011

Fisher, A. B., Chien, S., Barakat, A. I., & Nerem, R. M. (2001). Endothelial cellular response to altered shear stress. *American Journal of Physiology-Lung Cellular and Molecular Physiology*, *281*(3), L529-L533. https://doi.org/10.1152/ajplung.2001.281.3.L529

Formaggia, L., Quarteroni, A., & Veneziani, A. (Eds.). (2010). *Cardiovascular Mathematics: Modeling and simulation of the circulatory system* (Vol. 1). Springer Science & Business Media.

Gaidai, O., Cao, Y., & Loginov, S. (2023). Global cardiovascular diseases death rate prediction. *Current Problems in Cardiology*, *48*(5), 101622. https://doi.org/10.1016/j.cpcardiol.2023.101622

Girault, V., & Raviart, P. A. (1979). *Finite element approximation of the Navier-Stokes equations* (Vol. 749). Berlin: Springer.

Hecht. F. (2012). New development in FreeFem++. *Journal of Numerical Mathematics, 20*(3-4), 251-266. https://doi.org/10.1515/jnum-2012-0013

John, V. (2004). Reference values for drag and lift of a two-dimensional time-dependent flow around a cylinder. *International Journal for Numerical Methods in Fluids*, *44*(7), 777-788. https://doi.org/10.1002/fld.679

Kleinstreuer, C. (2016). *Biofluid dynamics: Principles and selected applications*. CRC Press.

Layton, W. (2008). *Introduction to the numerical analysis of incompressible viscous flows*. Society for Industrial and Applied Mathematics. https://doi.org/10.1137/1.9780898718904

Ma, L., Yan, C., & Yu, J. (2022). Suitability of an Artificial Viscosity Model for Compressible Under-Resolved Turbulence Using a Flux Reconstruction Method. *Applied Sciences*, *12*(23), 12272. https://doi.org/10.3390/app122312272

Manzari, M. T. (1999). An explicit finite element algorithm for convection heat transfer problems. *International Journal of Numerical Methods for Heat & Fluid Flow*, *9*(8), 860-877. https://doi.org/10.1108/09615539910297932

Margolin, L. G., & Lloyd-Ronning, N. M. (2023). Artificial viscosity—then and now. *Meccanica*, *58*(6), 1039-1052. https://doi.org/10.1007/s11012-022-01541-5

Nair, M. (2017). *Circulatory system. Fundamentals of anatomy and physiology for nursing and healthcare students* (2nd Ed.). Chichester: Wiley Blackwell.

Quarteroni, A., Veneziani, A., & Zunino, P. (2002). Mathematical and numerical modeling of solute dynamics in blood flow and arterial walls. *SIAM Journal on Numerical Analysis*, *39*(5), 1488-1511. https://doi.org/10.1137/S0036142900369714

Reneman, R. S., & Hoeks, A. P. (2008). Wall shear stress as measured in vivo: consequences for the design of the arterial system. *Medical & Biological Engineering & Computing*, *46*(5), 499-507. https://doi.org/10.1007/s11517-008-0330-2

Selmi, M., Belmabrouk, H., & Bajahzar, A. (2019). Numerical study of the blood flow in a deformable human aorta. *Applied Sciences*, *9*(6), 1216. https://doi.org/10.3390/app9061216

Sjösten, W., & Vadling, V. (2018). *Finite Element Approximations of 2D Incompressible Navier-Stokes Equations Using Residual Viscosity*. Uppsala Universitet.

Taylor, C. A., Petersen, K., Xiao, N., Sinclair, M., Bai, Y., Lynch, S. R., & Schaap, M. (2023). Patient-specific modeling of blood flow in the coronary arteries. *Computer Methods in Applied Mechanics and Engineering*, *417*(Part B), 116414. https://doi.org/10.1016/j.cma.2023.116414

Velten, K., Schmidt, D. M., & Kahlen, K. (2024). *Mathematical modeling and simulation: introduction for scientists and engineers*. John Wiley & Sons.

WHO (World Health Organization) (2019). Cardiovascular diseases (CVDs). (Accessed 11/06/2024) https://www.who.int/health-topics/cardiovascular-diseases#tab=tab_1